OPEN ACCESS Freely available online

PLOS ONE

Effects of Mechano-Electric Feedback on Scroll Wave Stability in Human Ventricular Fibrillation

Yuxuan Hu[1], Viatcheslav Gurev[2], Jason Constantino[1], Jason D. Bayer[1], Natalia A. Trayanova[1]*

1 Department of Biomedical Engineering, Johns Hopkins University, Baltimore, Maryland, United States of America, **2** Functional Genomics and Systems Biology, IBM T. J. Watson Research Center, Yorktown Heights, New York, United States of America

Abstract

Recruitment of stretch-activated channels, one of the mechanisms of mechano-electric feedback, has been shown to influence the stability of scroll waves, the waves that underlie reentrant arrhythmias. However, a comprehensive study to examine the effects of recruitment of stretch-activated channels with different reversal potentials and conductances on scroll wave stability has not been undertaken; the mechanisms by which stretch-activated channel opening alters scroll wave stability are also not well understood. The goals of this study were to test the hypothesis that recruitment of stretch-activated channels affects scroll wave stability differently depending on stretch-activated channel reversal potential and channel conductance, and to uncover the relevant mechanisms underlying the observed behaviors. We developed a strongly-coupled model of human ventricular electromechanics that incorporated human ventricular geometry and fiber and sheet orientation reconstructed from MR and diffusion tensor MR images. Since a wide variety of reversal potentials and channel conductances have been reported for stretch-activated channels, two reversal potentials, −60 mV and −10 mV, and a range of channel conductances (0 to 0.07 mS/μF) were implemented. Opening of stretch-activated channels with a reversal potential of −60 mV diminished scroll wave breakup for all values of conductances by flattening heterogeneously the action potential duration restitution curve. Opening of stretch-activated channels with a reversal potential of −10 mV inhibited partially scroll wave breakup at low conductance values (from 0.02 to 0.04 mS/μF) by flattening heterogeneously the conduction velocity restitution relation. For large conductance values (>0.05 mS/μF), recruitment of stretch-activated channels with a reversal potential of −10 mV did not reduce the likelihood of scroll wave breakup because Na channel inactivation in regions of large stretch led to conduction block, which counteracted the increased scroll wave stability due to an overall flatter conduction velocity restitution.

Citation: Hu Y, Gurev V, Constantino J, Bayer JD, Trayanova NA (2013) Effects of Mechano-Electric Feedback on Scroll Wave Stability in Human Ventricular Fibrillation. PLoS ONE 8(4): e60287. doi:10.1371/journal.pone.0060287

Editor: Alena Talkachova, University of Minnesota, United States of America

Received January 15, 2013; **Accepted** February 25, 2013; **Published** April 3, 2013

Funding: This project was supported by National Institutes of Health grant R01-HL103428, National Science Foundation grants CBET-0933029 and IOS-1124804 and NIH fellowship F31-HL103090. The funders had no role in study design, data collection and analysis, decision to publish, or preparation of the manuscript.

Competing Interests: Natalia A. Trayanova is a cofounder of CardioSolv, LLC. CardioSolv was not involved in this research. Viatcheslav Gurev is employed by the IBM T.J. Watson Research Center. There are no patents, products in development or marketed products to declare. This does not alter the authors' adherence to all the PLOS ONE policies on sharing data and materials.

* E-mail: ntrayanova@jhu.edu

Introduction

Experimental and clinical research has demonstrated that the mechanical environment of the heart, in health and disease, is capable of exerting influence on cardiac electrophysiology [1]. Temporal changes in strain take place during all phases of the cardiac cycle. Abnormal electrical propagation during arrhythmias also leads to abnormal strain distributions in the heart, which in turn could affect electrical propagation. The mechanisms that contribute to strain-dependent modulation of electrical wave propagation are termed mechano-electric feedback (MEF) mechanisms [2].

There are several MEF mechanisms in the heart, including stretch-induced changes in intracellular Ca handling [3], depolarization of cardiac fibroblasts by stretch (via mechano-sensitive ion channels) affecting the resting potential and action potential duration (APD) of the coupled myocyte [4], and most importantly, myocyte sarcolemmal channel activation by mechanical stimuli [5,6]. Stretch-activated channels (SAC), a type of mechanically activated ionic channels identified in cardiac tissue, have been found responsible for the generation of arrhythmias following an appropriately timed mechanical impact to the heart (commotio cordis) [7,8], as well for the termination of ventricular arrhythmias following a precordial thump [9]. Abnormal deformation associated with the establishment of arrhythmia can also affect the progression of the arrhythmia itself; this aspect of MEF has received less attention in the literature.

On one hand, opening of SAC has been demonstrated to depolarize the resting membrane and thus cause Na channel inactivation [10,11], which can stabilize scroll waves [12], the waves that underlie reentrant arrhythmias. On the other hand, SAC-induced depolarization and Na channel inactivation have been shown to give rise to scroll wave breakup [13] that increases electrical instability and leads to turbulent behavior underling the most lethal arrhythmias. These contradictory results indicate that the conditions under which and the mechanisms by which recruitment of SAC alters scroll wave stability remain incompletely understood.

To provide a comprehensive understanding of the mechanisms by which SAC opening affects the stability of scroll waves, it is

necessary to record, in 3D, both the electrical and mechanical activity simultaneously, and at a high spatiotemporal resolution. Currently, this is not possible by means of experimentation. In contrast, biophysically-detailed computer simulations of electromechanical function at the organ scale have the capability to dissect the relationship between stretch and arrhythmia maintenance; initial attempts in this direction have already been made [14,15]. The latter simulation studies had focused predominantly on the effect of recruitment of SACs with large conductances and reversal potentials close to zero on scroll wave stability. However, SACs have been demonstrated to exhibit a wide variety of reversal potentials and conductances [5]. Opening of SAC with a reversal potential close to the resting membrane potential has been shown to shorten APD [16], while opening of SAC with a less negative reversal potential has been found to have the opposite effect, resulting in APD prolongation [17]. The degree of lengthening or shortening of APD is affected by SAC conductance as well. Since recruitment of SAC with different reversal potentials and conductances leads to different electrophysiological changes in cardiac myocytes, it is thus possible that SAC opening could affect scroll wave stability in the 3D heart via different mechanisms depending on the channel population characteristics.

The goal of this study was to conduct a comprehensive analysis of the effects of SAC recruitment on scroll wave stability in the fibrillating ventricles. To achieve this goal, a strongly-coupled MRI-based biophysically-detailed electromechanics model of the human ventricles was developed. We used this model (1) to test the hypothesis that recruitment of SAC affects scroll wave stability differently depending on the reversal potential and channel conductance of SAC and (2) to uncover the relevant mechanisms underlying the different behaviors.

Materials and Methods

Electromechanical Model

The image-based 3D electromechanical model of the human ventricles developed for this study as shown in Figure 1A incorporates realistic ventricular geometry and fiber-sheet architecture reconstructed from high-resolution magnetic resonance (MR) and diffusion tensor MR images [18]. The model consists of an electrical and a mechanical component (Figure 1B), which are coupled via the intracellular calcium dynamics [19,20].

Mathematical description of the electrical component of the model was based on the monodomain representation of cardiac tissue; our group has made extensive use of such large-scale electrophysiological models of the heart [21]. Membrane kinetics were represented by the ten Tusscher et al. ionic model of the human ventricular myocyte [22]. To make the substrate prone to arrhythmia, the maximum conductances of the IKr, IKs, IpCa, and IpK currents and the time constant for the f gate of the L-type calcium current were modified throughout the ventricles, as described in [23], producing a steep local APD restitution curve with a maximum slope of 1.8.

The mechanical component incorporated a continuum mechanics model of the ventricles and a lumped-parameter model of the circulatory system, both of which have been described previously [19]. The parameters in the circulatory system model were adjusted for the human ventricles using available physiological data [24]; parameter values are presented in the Supporting Information Table S1. Active tension generation in the mechanics component was represented by the Rice et al. model of myofilament dynamics [25]. To simulate reduced contractility during arrhythmias, the half-activation constant for shift of a regulatory unit to a permissive state in the Rice et al. model was increased by 20% to decrease the sensitivity of troponin to Ca; this ensured that the maximal pressure during ventricular fibrillation (VF) matched that observed clinically [26].

The electrical mesh consisted of 4274379 elements with a spatial resolution of 500 μm; our electrical meshes are always tested for convergence (for the specific solvers we used; descriptions can be found in [27]). Description of the electrical mesh generation procedure can be found in Prassl et al. [28] The mechanical mesh [19] was a nonlinear mesh with 230 hexahedral elements. The spatial resolution for the mechanical mesh was 10 mm. The methodology for the generation of the mechanical mesh is described in Gurev et al [19].

The electrical and mechanical components of the model were strongly coupled. A mechanical solution step (500 μs) followed every five electrical solution steps (100 μs). During electrical propagation, the spatial distribution of intracellular Ca concentration throughout the ventricles was calculated from the ionic model at each node in the electrical component computational mesh and then, at every fifth solution step, mapped onto the Gaussian points in the mechanical computational mesh. At every Gaussian point, the local intracellular Ca concentration was inputted into the myofilament model to generate the local active tension. After solving for the mechanical deformation of the ventricles arising from the active tension, strain tensors were mapped back onto the nodes in the electrical computational mesh. From the strain tensor at each node, the local stretch ratio in the fiber direction was determined and used to calculate the local SAC current (see below for formulation) at that node, which in turn affected global propagation. The electromechanical model detailed above has been extensively validated by our group using electromechanical wave imaging [29]. Numerical approaches to solving the equations of the electromechanical model used methodologies described elsewhere [19,30]. This state-of-the-art human electromechanical model is of broad applicability and can be used in a wide range of studies in cardiac electromechanics.

MEF

Consistent with the goal of the study, SACs were incorporated in the electromechanical model of the human ventricles; opening of SAC was the mechanism by which mechanical deformation provided feedback into the electrical activity of the heart. The possible effect of mechanical deformation on geometry was not incorporated into the model to decrease model complexity and because it has been demonstrated to not affect scroll wave stability [15]. Since the current through SAC, I_{SAC}, has been shown to increase linearly with stretch [17], I_{SAC} was formulated as being linearly proportional to the stretch ratio in the fiber direction, λ_f:

$$I_{SAC} = g_{SAC}(\lambda_f - 1)(V_m - V_{SAC}) \text{ if } \lambda_f > 1$$

$$I_{SAC} = 0 \text{if } \lambda_f \leq 1 \quad (1)$$

where V_m is the transmembrane potential, and V_{SAC} is the reversal potential of SAC. SACs were assumed to conduct only when λ_f was larger than 1 [31]; thus, I_{SAC} was zero during myofiber shortening. Since I_{SAC} is the total current through both non-selective cation and potassium-conducting SACs, the value of V_{SAC} depends on the degree of the relative expressions of non-selective cation and potassium-conducting channels in myocardial tissue. Given that non-selective cation SACs have been reported to have a reversal potential of 0 mV [32] and potassium-conducting SACs operate with a reversal potential of −90 mV [33], V_{SAC} can

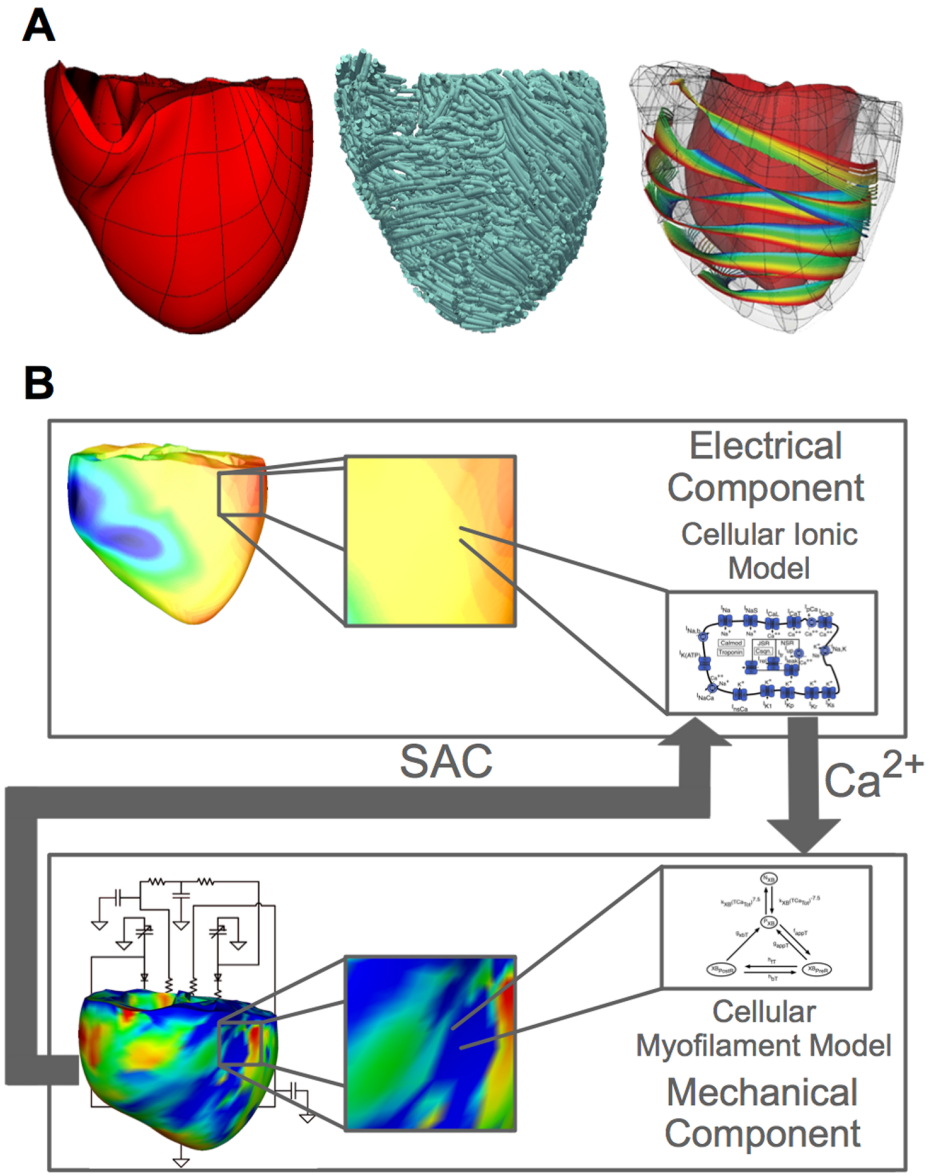

Figure 1. MRI-based electromechanical model of the human ventricles. (A): The mechanical mesh, fiber orientation and sheet structure of the human ventricular model. (B): The schematic diagram of the electromechanical model.
doi:10.1371/journal.pone.0060287.g001

range between −90 mV and 0 mV. In this study, we used two values of V_{SAC} that spanned that range, one close to the membrane resting potential (−60 mV [34]) and another less negative (−10 mV [17]). The SAC conductance g_{SAC} was varied between 0 and 0.07 mS/μF [1,35,36] to fully investigate the effects of SAC recruitment on scroll wave stability.

VF Induction Protocol

To induce VF, the ventricles were first paced seven times from the apex at a 700 ms basic cycle length to achieve steady-state propagation. Then, at 500 ms following the last pacing beat, a cross-field stimulation was applied to the posterior side of the ventricles, inducing reentry. Reentrant waves broke up due to the restitution properties of the myocardium, leading to VF. Simulations were run for 5 seconds post-VF induction to ensure that VF was sustained.

Scroll-wave Filaments and Pseudo ECGs

To analyze the stability of the scroll waves, the number of scroll-wave filaments (the organizing centers of reentry) throughout the ventricular volume was determined at time instants 200 ms apart during 4 seconds of simulation using an algorithm based on phase angle maps, as described previously [37].

Pseudo ECGs were computed as follows [38]:

$$ECG = \int_V \frac{D\nabla V_m \cdot \vec{r}}{r^3} dV \qquad (2)$$

where V is the ventricular volume, $\bar{r}$ is the vector from each point in the ventricular volume to the recording electrode, the latter placed 10 cm from the center of the anterior wall of the ventricles in the anterior direction of the transverse plane, as done previously

[14], and r is the distance from each point in the ventricular volume to the recording electrode.

Results

VF in the Electromechanical Model without SAC Representation

Figure 2 presents the epicardial transmembrane potential distribution maps of sustained VF (Figure 2A) in the model without SAC representation; scroll waves break up continuously, maintaining VF (a Supplementary Movie (S1) is available in Supporting Information). There are multiple scroll wave filaments present in the ventricles during the simulation (Figure 2B). The irregular and complex pseudo-ECG (Figure 2C) is a manifestation of the numerous meandering reentrant waves sustaining VF.

Inclusion of SAC with V_{SAC} of −60 mV Results in Partial Suppression of Scroll Wave Breakup by Flattening of the APD Restitution Curve

Comparing the number of filaments in the model with and without SAC (V_{SAC} of −60 mV) revealed that SAC activation partially suppressed (but did not eliminate) scroll wave breakup for all values of g_{SAC}. Indeed, for the model with SAC, the average number of filaments decreased by 46–62%, depending on the value of g_{SAC}, as compared to the model without SAC (Table 1A).

Table 1. The average number of filaments in the VF human ventricular electromechanical model with SAC of V_{SAC} of −60 mV for different g_{SAC}.

	Average No. of filaments
Without SAC	7.6±2.2
g_{SAC} (mS/μF)	
0.03	2.9±1.0*
0.05	3.1±1.7*
0.07	4.1±1.7*

The symbol * indicates that the average number of filaments is significantly smaller than that in the model without SAC representation ($p<0.05$).
doi:10.1371/journal.pone.0060287.t001

To understand the mechanisms by which recruitment of SAC with V_{SAC} of −60 mV decreased the likelihood of scroll wave breakup, we first investigated an important determinant of dynamic instability, the single cell APD restitution relation and its modification by MEF. Single cell APD restitution relations with SAC recruitment were calculated for the three values of g_{SAC} examined; results are presented in Figure 3. The strain map of the fibrillating human heart at each time instant during the simulation was analyzed (a representative strain map is shown in Figure 4A)

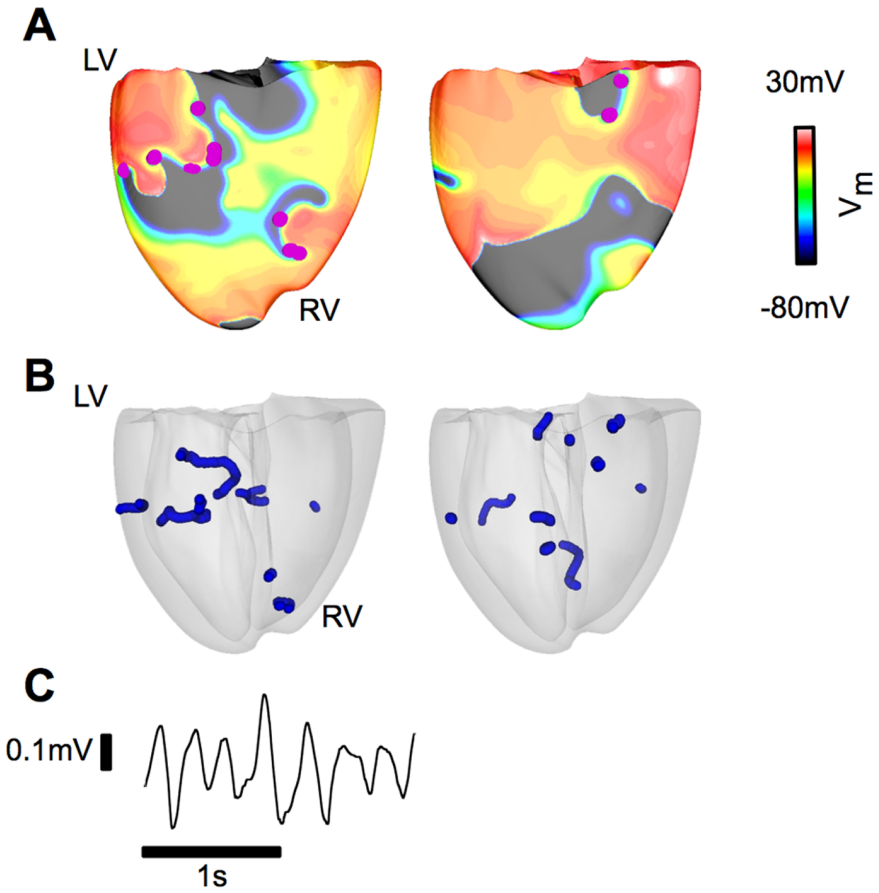

Figure 2. VF in the electromechanical model without SAC representation. (A): Epicardial transmembrane potential distribution maps on the posterior wall from the simulation without SAC representation. Pink dots indicate the locations of the phase singularities. (B): Posterior semi-transparent view of the ventricles shows the filament distribution (blue). (C): Pseudo-ECG.
doi:10.1371/journal.pone.0060287.g002

and the maximum λ_f was found to be 1.5. Single-cell APD restitution curves were thus constructed for different degrees of SAC opening corresponding to λ_f values from 1.0 to 1.5. As shown in Figure 3, current through SAC leads to flattening of the single-cell APD restitution curve for all values of λ_f and g_{SAC}. The larger the value of λ_f or g_{SAC}, the flatter the resulting APD restitution curve.

At any time instant during VF, the distribution of λ_f in the ventricles was heterogeneous, as illustrated by the snapshot map in Figure 4A. This led to non-uniform I_{SAC} throughout the ventricles, which in turn gave rise to varying degrees of APD restitution flattening in the ventricular model with SAC. A map of the distribution of maximum restitution slope in the ventricles for g_{SAC} of 0.07 mS/μF is presented in Figure 4B. Regions of large λ_f had maximum restitution slopes smaller than 1, whereas regions of small λ_f had maximum restitution slopes larger than 1 but less than the original value of 1.8. These regional differences in the restitution-flattening effect of SAC opening are the reason why scroll waves continued to break up (albeit much less frequently). Should λ_f have been homogeneous and of value 1.2 or above, recruitment of SAC with V_{SAC} of −60 mV would have led to the conversion of VF into ventricular tachycardia, as our simulations found; Figure 4C shows a stable scroll-wave with a single filament throughout the simulation in this case (for $\lambda_f = 1.2$ everywhere).

Recruitment of SAC with V_{SAC} of −10 mV Diminishes Scroll Wave Breakup at Low g_{SAC}, but not at Large g_{SAC}

Comparing the number of filaments that sustain VF in the ventricular model with and without SAC demonstrated that recruitment of SAC with V_{SAC} of −10 mV had a different effect on the stability of scroll waves depending on the value of g_{SAC}. For low values of g_{SAC} (from 0.02 mS/μF to 0.04 mS/μF), the average number of filaments for the model with SAC decreased by 32–51% compared to that in the model without SAC (Table 2A), indicating less frequent scroll wave breakup. For large values of g_{SAC} (0.05 mS/μF and above), the average number of filaments for the model with SAC was not significantly different from that in the model without SAC (Table 2A), demonstrating that scroll wave breakup was not suppressed.

To understand the mechanisms by which opening of SAC with V_{SAC} of −10 mV diminishes scroll wave breakup at low g_{SAC}, we first determined the single cell APD restitution curves with SAC recruitment in this case and found that opening of SAC with V_{SAC} of −10 mV does not change the single cell APD restitution curves. Since previous studies have shown that flattening of conduction velocity (CV) restitution curves also leads to stabilization of scroll waves [39,40], we next determined the CV restitution curves with SAC recruitment for all g_{SAC} values using a model of a slab of human ventricular tissue as done previously [41]. The results for three representative g_{SAC} values, 0.02, 0.04 and 0.07 mS/μF, are shown in Figure 5. Analysis of the ventricular strain maps for all time instants showed that in this case the maximum λ_f was also 1.5, despite the differences in the spatial distribution of strain. Thus, CV restitution curves were constructed for different degrees of SAC opening corresponding to λ_f of 1.0, 1.2, 1.4 and 1.5. As demonstrated in Figure 5A–C, current through SAC leads to flattening of the CV restitution curves for all values of λ_f and g_{SAC}. The larger the value of λ_f or g_{SAC}, the flatter the CV restitution curve.

Heterogeneous distribution of λ_f throughout the ventricles as demonstrated in Figure 4A gave rise to different degrees of SAC opening and thus CV restitution curve flattening. The flatter CV restitution curve in regions of substantial stretch resulted in suppression of scroll wave breakup there; the still-steep CV restitution curve in regions of minimal stretch continued to promote scroll wave breakup. As a result, the degree of spiral wave breakup and thus the number of filaments in the ventricles diminished. If the distribution of λ_f (of value 1.2 or above) were homogeneous, opening of SAC with V_{SAC} of −10 mV would have completely suppressed scroll wave breakup, as shown by the stable scroll waves throughout the simulation in Figure 5D (for $\lambda_f = 1.2$ everywhere).

For large values of g_{SAC}, opening of SAC with V_{SAC} of −10 mV in regions of substantial stretch (Figure 6A) resulted in a large inward I_{SAC} during repolarization (Figure 6C), which elevated the resting membrane potential from −85 mV in the model without SAC to −77 mV in the ventricles with SAC (Figure 6E) and thus inactivated the Na channels in the latter model (Figure 6D). As a result, conduction block occurred in regions of substantial stretch (Figure 6E) causing scroll wave breakup there (Figure 6B). The scroll wave breakup in regions of substantial stretch counteracted the increased scroll wave stability due to a flatter CV restitution there (Figure 5C), explaining why the number of scroll wave filaments in the model with SAC was not significantly different from that in the model without SAC at large values of g_{SAC}.

Discussion

This study investigated the effects of SAC opening on scroll wave stability in the fibrillating ventricles by employing a strongly-coupled MRI-based anatomically accurate 3D model of human ventricular electromechanics. A comprehensive analysis of how recruitment of SAC influences scroll wave breakup was performed for different SAC reversal potentials and channel conductances.

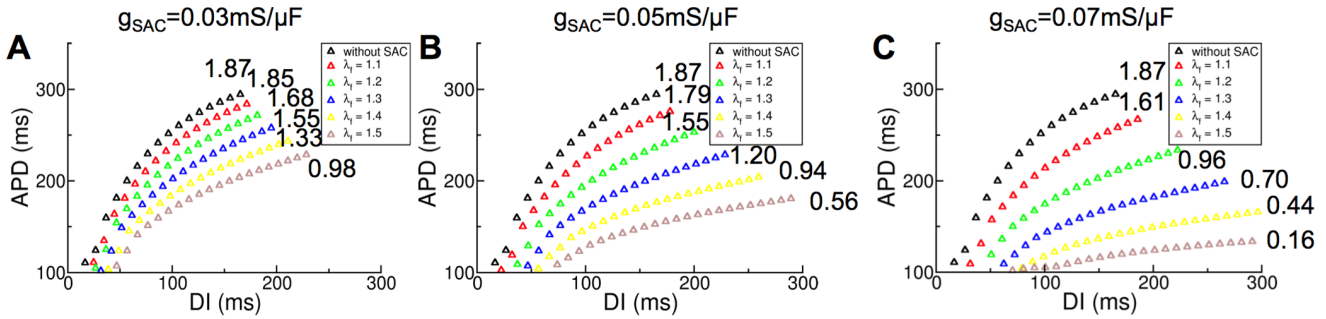

Figure 3. Recruitment of SAC with V_{SAC} of −60 mV flattens the single-cell APD restitution curve. Changes in the single-cell APD restitution curves due to SAC opening for different values of λ_f. (A): g_{SAC} = 0.03 mS/μF, (B): g_{SAC} = 0.05 mS/μF and (C): g_{SAC} = 0.07 mS/μF.
doi:10.1371/journal.pone.0060287.g003

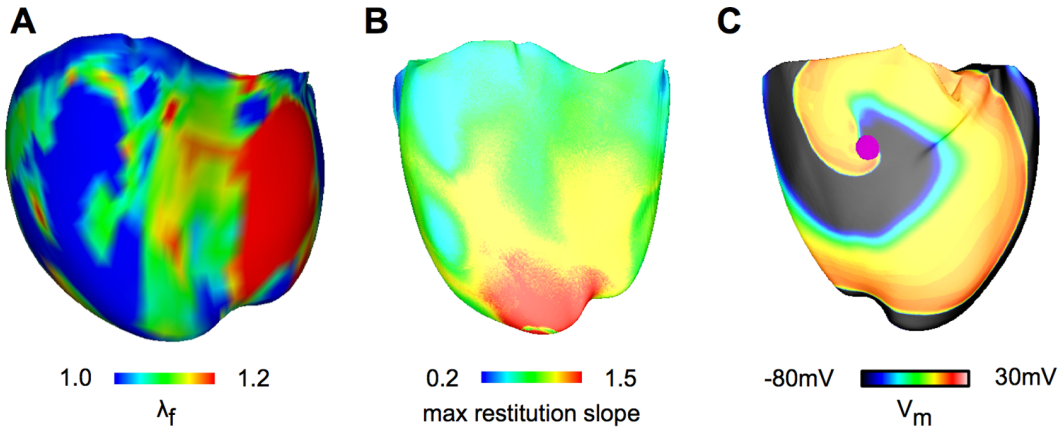

Figure 4. Recruitment of SAC with V_{SAC} of −60 mV diminishes scroll wave breakup. (A): Snapshot of the heterogeneous λ_f distribution at 2.3 s after arrhythmia induction for the ventricular model with V_{SAC} of −60 mV; g_{SAC} = 0.07 mS/μF. In plotting the λ_f distribution, the range 1.0 to 1.2 was chosen for visual purposes, as 90% of the data points fell within this range. (B): Maximum APD restitution slope distribution for the same model and time instant as in (A). In plotting of maximum APD restitution slopes, the range 0.2 to 1.5 was chosen for visual purposes, as 97% of the data points fell within this range. (C): Epicardial transmembrane potential distribution map on the anterior wall for V_{SAC} of −60 mV and g_{SAC} of 0.07 mS/μF when λ_f was assumed constant and equal to 1.2. Pink dot indicates the location of the phase singularity.
doi:10.1371/journal.pone.0060287.g004

We discovered that recruitment of SAC affects scroll wave stability via different mechanisms depending on the reversal potential and channel conductance of SAC.

1. Opening of SAC with V_{SAC} of −60 mV decreases the likelihood of scroll wave breakup for all values of g_{SAC}. The underlying mechanism is flattening of the APD restitution curve in regions of high strain.
2. Opening of SAC with V_{SAC} of −10 mV partially inhibits scroll wave breakup at low values of g_{SAC} by flattening the CV restitution relation in regions of high stretch. For large values of g_{SAC}, recruitment of SAC with V_{SAC} of −10 mV did not diminish the likelihood of scroll wave breakup because Na channel inactivation in regions of large stretch (as a result of SAC opening) led to conduction block and thus scroll wave breakup, which counteracted the increased scroll wave stability due to a flatter CV restitution.

Table 2. The average number of filaments in the ventricular model with SAC of V_{SAC} of −10 mV for different g_{SAC}.

	Average No. of filaments
Without SAC	7.6±2.2
g_{SAC} (mS/μF)	
0.01	7.3±3.1
0.02	4.4±1.6*
0.03	3.7±1.0*
0.04	5.2±2.1*
0.05	7.4±1.3
0.06	8.0±2.8
0.07	8.9±2.4

The symbol * indicates that the average number of filaments is significantly smaller than that in the model without SAC representation ($p<0.05$).
doi:10.1371/journal.pone.0060287.t002

The MRI-based Electromechanical Model of the Human Ventricles

In this study, we present a strongly-coupled MRI-based model of human cardiac electromechanics. This new model incorporates reconstructions of human ventricular geometry and fiber orientation from MR and diffusion tensor MR images, which allows for simulation of realistic ventricular deformation during arrhythmias. The circulatory model to which it is coupled is adapted for the human ventricles, enabling accurate representation of hemodynamic changes during arrhythmia. The implementation of strong coupling in our electromechanical model allows for the dynamic inclusion of the effect of MEF in the electrical component since a mechanical solution step was performed following every fifth electrical solution step; this allows for a more accurate simulation of the effect of MEF compared to what has been done previously, where a mechanical solution step followed every 100 electrical solution steps [14]. This is the first electromechanical model to incorporate MEF in this manner. The simulations performed using this model in the present study represent a comprehensive evaluation of the electromechanical behavior of the human ventricles in VF and of the effect of SAC opening on arrhythmia stability.

Alteration of Cellular Electrophysiological Properties by MEF

Recruitment of non-selective cation SAC results in prolongation of APD with a crossover during systole, where the early phase of repolarization is shortened and the late phase prolonged [10,32]. Opening of potassium-conducting SAC causes repolarization during systole and results in APD shortening [16]. Thus, the combined electrophysiological effect of the opening of the two different SACs can vary depending on the degree of expression of non-selective cation SAC and potassium-conducting SAC in myocardial tissue; experimental observations have shown both prolongation [17,32,42] and shortening of APD or monophasic action potential [43,44].

Single cell behavior in our models is consistent with this experimental data, as SAC opening with V_{SAC} at −60 mV, which represented a higher degree of expression of potassium-conducting SAC, produced shortening of APD. SAC opening with V_{SAC} at

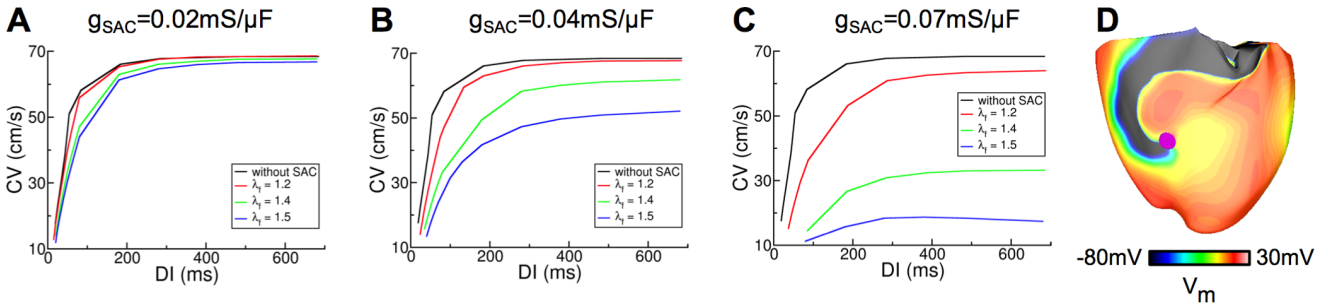

Figure 5. Recruitment of SAC with V_{SAC} of −10 mV diminishes scroll wave breakup at low g_{SAC}. Changes in the CV restitution curves due to SAC opening for different values of λ_f. (A): g_{SAC} = 0.02 mS/μF, (B): g_{SAC} = 0.04 mS/μF and (C): g_{SAC} = 0.07 mS/μF. (D): Epicardial transmembrane potential distribution map on the anterior wall for V_{SAC} of −10 mV and g_{SAC} = 0.04 mS/μF when λ_f was assumed constant and equal to 1.2. Pink dot indicates the location of the phase singularity.
doi:10.1371/journal.pone.0060287.g005

−10 mV, which represented a higher degree of expression of non-selective cation SAC, resulted in APD prolongation with a crossover and elevation of resting potential. Different conductances have been reported for SAC as well [5]; we showed that the degree of lengthening or shortening of APD is affected by SAC conductance. Since recruitment of SAC with different reversal potentials and conductances leads to different electrophysiological changes in cardiac myocytes, it was important to incorporate different degrees of expression of the two types of SAC when examining the whole-heart behavior, extending the findings of an earlier study [14].

Effects of MEF on CV

While examining the dependence of CV on strain was not the subject of this study, this relationship affected the dependence of the CV restitution on MEF, and thus indirectly spiral wave behavior in the model. Previous studies have shown that for a wide range of pacing cycle lengths, the CV can exhibit biphasic; constant; increasing; and decreasing relationship with respect to strain (see review [11]). Our results are consistent with these seemingly disparate findings: we found that CV displays different relationships with respect to stretch depending on pacing cycle length, g_{SAC}, and V_{SAC}. Opening of SAC with V_{SAC} of −10 mV resulted in independence of CV on stretch for low values of g_{SAC} and in a decrease in CV with the increase in stretch for large values of g_{SAC} at all pacing cycle lengths. For low values of g_{SAC}, opening of SAC with V_{SAC} of −10 mV produced a small inward I_{SAC} during repolarization, which did not lead to large elevation in the resting membrane potential and thus did not inactivate Na channels and reduce CV. For large values of g_{SAC}, recruitment of SAC with V_{SAC} of −10 mV resulted in a larger I_{SAC}, which was sufficient to inactivate Na channels and thus slow conduction. Recruitment of SAC with V_{SAC} of −60 mV resulted in the increase in CV with increasing stretch at short pacing cycle lengths (400 ms and below) and in a CV unaltered with stretch at long pacing cycle lengths (between 400 and 1000 ms) for all values of g_{SAC}. Opening of SAC with V_{SAC} of −60 mV shortened APD and thus increased DI. At short pacing cycle lengths, the increase in DI led to a better recovery from refractoriness and thus increased CV, whereas at large pacing cycle lengths, there was already a full recovery from refractoriness without SAC opening and thus the increase in DI did not increase CV.

Effect of SAC Recruitment on Scroll Wave Stability

There has been a significant body of research on the determinants of scroll wave stability. APD and CV restitution relationships have been found to be two main determinants of scroll wave stability; a flat APD or CV restitution curve was shown to lead to stable scroll waves, whereas a steep APD or CV restitution relation gives rise to scroll wave breakup [39,45,46]. Studies concerning determinants of scroll wave stability have mainly been electrophysiological without taking into account the effect of mechanical contraction of the ventricles on scroll wave stability. However, heterogeneity in strain throughout the ventri-

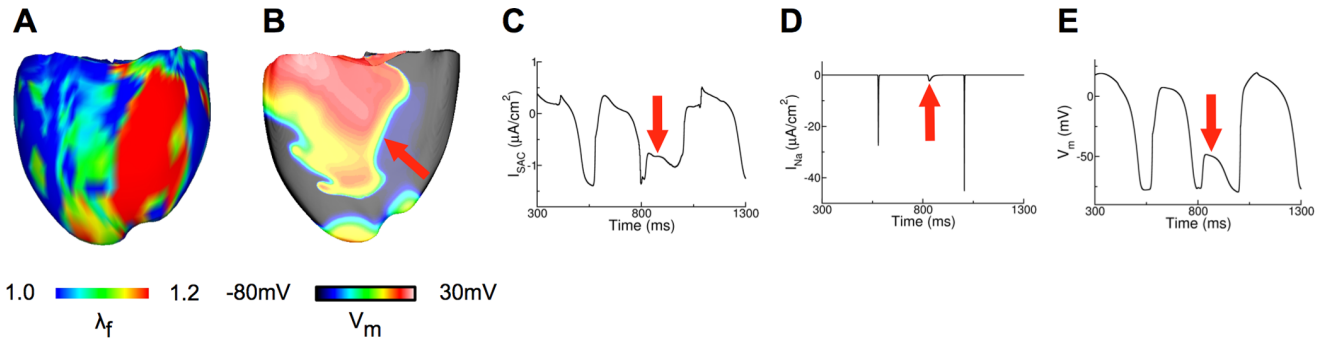

Figure 6. Recruitment of SAC with V_{SAC} of −10 mV results in scroll wave breakup at large g_{SAC}. (A): Distribution of λ_f at 0.9 s after arrhythmia induction for the ventricular model with V_{SAC} of −10 mV; g_{SAC} = 0.07 mS/μF. (B): Scroll wave breakup in the region of large stretch (indicated by arrow). (C), (D) and (E) are plots of I_{SAC}, I_{Na} and V_m, respectively from the node indicated by the arrow in (B). The arrow denotes in (C): the large inward I_{SAC} during repolarization, in (D): inactivation of Na channels, (E): conduction block.
doi:10.1371/journal.pone.0060287.g006

cles, especially during VF, leads to heterogeneous MEF via SAC opening, which affects scroll wave stability. Since experimental studies require contraction to be blocked to reduce movement artifacts from optical mapping recording [47], realistic modeling offers a means to explore how mechanical contraction of the ventricles affects scroll wave stability via MEF.

We showed that opening of SAC with V_{SAC} of -60 mV diminished scroll wave breakup by flattening the APD restitution curve. Our findings are consistent with experimental results on scroll wave stability in the presence of the drug D600 (a calcium channel blocker at low concentrations), which caused acceleration of repolarization and shortening of APD, effects similar to those of SAC opening with V_{SAC} of -60 mV: D600 similarly promoted scroll wave stability by flattening the APD restitution curve [13].

We also demonstrated that opening of SAC with V_{SAC} of -10 mV partially inhibits scroll wave breakup at low values of g_{SAC} by flattening the CV restitution relation in regions of high stretch. Previous studies have shown that slowing of scroll wave rotation leads to stabilization of scroll waves [23,48,49]; the mechanism is that the period of rotation and thus the diastolic interval increase, resulting in the operational regime being in the less steep part of the APD restitution curve [48,49]. This indirect suppression of scroll wave breakup is also present in our simulation results, as Na channels were inactivated with opening of SAC with V_{SAC} of -10 mV and thus scroll wave rotation was slowed.

For large values of g_{SAC}, recruitment of SAC with V_{SAC} of -10 mV did not diminish the likelihood of scroll wave breakup because Na channel inactivation in regions of large stretch as a result of SAC opening led to conduction block and thus scroll wave breakup, which counteracted the increased scroll wave stability due to a flatter CV restitution. This is consistent with results obtained by Keldermann et al.'s [14]. Since Keldermann et al. evaluated the effect of large SAC conductances only, the destabilizing effect of SAC opening on scroll waves was the dominant mechanism. The study by Kuijpers et al. [50] demonstrated that in the atria, Na channel inactivation as a result of SAC opening leads to functional block, thereby terminating arrhythmias. The fact that Na channel inactivation as a result of SAC opening led to scroll wave breakup in the ventricles, whereas in atria it led to termination of arrhythmias might be due to the fact that atria have less tissue for propagation compared to the ventricles. Atria, unlike the ventricles, may not be able to support an alternative pathway circumventing the conduction block that is long enough, compared to the wavelength, to result in the establishment of a sustained reentry.

The results of the study demonstrate the possible therapeutic potential of SAC recruitment during VF, indicating that clinical strategies could be devised to minimize scroll wave breakup. For instance, gene therapy could be designed and tested to increase the expression of potassium-conducting SACs, so that g_{SAC} would be increased while V_{SAC} is brought closer to the myocyte resting potential. This will bring SACs to a regime that maximizes the suppression of scroll wave breakup.

Study Limitations

Previous experiments have shown that SAC conductance can be a function of strain rate [51,52]. However, this limitation would not greatly affect our results since it was previously shown that regions with larger strains were associated with larger strain rates [53]. SAC was assumed to be uniformly distributed in the ventricles. Such assumption was made due to lack of experimental studies on this subject.

Supporting Information

Table S1 Adjusted parameters of the Kerckhoffs et al. circulatory model.
(DOCX)

Movie S1 VF in the ventricular model without SAC representation.
(MP4)

Author Contributions

Conceived and designed the experiments: YH JDB VG NAT. Performed the experiments: YH. Analyzed the data: YH. Contributed reagents/materials/analysis tools: YH JC VG. Wrote the paper: YH JDB JC NAT.

References

1. Kohl P, Hunter P, Noble D (1999) Stretch-induced changes in heart rate and rhythm: clinical observations, experiments and mathematical models. Prog Biophys Mol Biol 71: 91–138.
2. Kohl P, Ravens U (2003) Cardiac mechano-electric feedback: past, present, and prospect. Prog Biophys Mol Biol 82: 3–9.
3. Xie LH, Sato D, Garfinkel A, Qu Z, Weiss JN (2008) Intracellular Ca alternans: coordinated regulation by sarcoplasmic reticulum release, uptake, and leak. Biophys J 95: 3100–3110.
4. Miragoli M, Gaudesius G, Rohr S (2006) Electrotonic modulation of cardiac impulse conduction by myofibroblasts. Circ Res 98: 801–810.
5. Hu H, Sachs F (1997) Stretch-activated ion channels in the heart. J Mol Cell Cardiol 29: 1511–1523.
6. Baumgarten CM, Clemo HF (2003) Swelling-activated chloride channels in cardiac physiology and pathophysiology. Prog Biophys Mol Biol 82: 25–42.
7. Link MS, Wang PJ, VanderBrink BA, Avelar E, Pandian NG, et al. (1999) Selective activation of the K(+)(ATP) channel is a mechanism by which sudden death is produced by low-energy chest-wall impact (Commotio cordis). Circulation 100: 413–418.
8. Li W, Kohl P, Trayanova N (2004) Induction of ventricular arrhythmias following mechanical impact: a simulation study in 3D. J Mol Histol 35: 679–686.
9. Li W, Kohl P, Trayanova N (2006) Myocardial ischemia lowers precordial thump efficacy: an inquiry into mechanisms using three-dimensional simulations. Heart Rhythm 3: 179–186.
10. Zabel M, Koller BS, Sachs F, Franz MR (1996) Stretch-induced voltage changes in the isolated beating heart: importance of the timing of stretch and implications for stretch-activated ion channels. Cardiovasc Res 32: 120–130.
11. McNary TG, Sohn K, Taccardi B, Sachse FB (2008) Experimental and computational studies of strain-conduction velocity relationships in cardiac tissue. Prog Biophys Mol Biol 97: 383–400.
12. Kawase A, Ikeda T, Nakazawa K, Ashihara T, Namba T, et al. (2003) Widening of the excitable gap and enlargement of the core of reentry during atrial fibrillation with a pure sodium channel blocker in canine atria. Circulation 107: 905–910.
13. Wu TJ, Lin SF, Weiss JN, Ting CT, Chen PS (2002) Two types of ventricular fibrillation in isolated rabbit hearts: importance of excitability and action potential duration restitution. Circulation 106: 1859–1866.
14. Keldermann RH, Nash MP, Gelderblom H, Wang VY, Panfilov AV (2010) Electromechanical wavebreak in a model of the human left ventricle. Am J Physiol Heart Circ Physiol 299: H134–143.
15. Panfilov AV, Keldermann RH, Nash MP (2007) Drift and breakup of spiral waves in reaction-diffusion-mechanics systems. Proc Natl Acad Sci U S A 104: 7922–7926.
16. Van Wagoner DR (1993) Mechanosensitive gating of atrial ATP-sensitive potassium channels. Circ Res 72: 973–983.
17. Zeng T, Bett GC, Sachs F (2000) Stretch-activated whole cell currents in adult rat cardiac myocytes. Am J Physiol Heart Circ Physiol 278: H548–557.
18. Vadakkumpadan F, Arevalo H, Prassl AJ, Chen J, Kickinger F, et al. (2010) Image-based models of cardiac structure in health and disease. Wiley Interdiscip Rev Syst Biol Med 2: 489–506.
19. Gurev V, Lee T, Constantino J, Arevalo H, Trayanova NA (2011) Models of cardiac electromechanics based on individual hearts imaging data: image-based electromechanical models of the heart. Biomech Model Mechanobiol 10: 295–306.
20. Constantino J, Hu Y, Trayanova NA (2012) A computational approach to understanding the cardiac electromechanical activation sequence in the normal

and failing heart, with translation to the clinical practice of CRT. Prog Biophys Mol Biol.
21. Moreno JD, Zhu ZI, Yang PC, Bankston JR, Jeng MT, et al. (2011) A computational model to predict the effects of class I anti-arrhythmic drugs on ventricular rhythms. Sci Transl Med 3: 98ra83.
22. ten Tusscher KH, Noble D, Noble PJ, Panfilov AV (2004) A model for human ventricular tissue. Am J Physiol Heart Circ Physiol 286: H1573–1589.
23. ten Tusscher KH, Panfilov AV (2006) Alternans and spiral breakup in a human ventricular tissue model. Am J Physiol Heart Circ Physiol 291: H1088–1100.
24. Klingensmith ME, Chen LE, Glasgow SC, Goers TA, Melby SJ (2008) The Washington Manual of Surgery; Klingensmith ME, Chen LE, Glasgow SC, Goers TA, Melby SJ, editors.
25. Rice JJ, Wang F, Bers DM, de Tombe PP (2008) Approximate model of cooperative activation and crossbridge cycling in cardiac muscle using ordinary differential equations. Biophys J 95: 2368–2390.
26. Sharma AD, Bennett TD, Erickson M, Klein GJ, Yee R, et al. (1990) Right ventricular pressure during ventricular arrhythmias in humans: potential implications for implantable antitachycardia devices. J Am Coll Cardiol 15: 648–655.
27. Plank G, Zhou L, Greenstein JL, Cortassa S, Winslow RL, et al. (2008) From mitochondrial ion channels to arrhythmias in the heart: computational techniques to bridge the spatio-temporal scales. Philos Transact A Math Phys Eng Sci 366: 3381–3409.
28. Prassl AJ, Kickinger F, Ahammer H, Grau V, Schneider JE, et al. (2009) Automatically generated, anatomically accurate meshes for cardiac electrophysiology problems. IEEE Trans Biomed Eng 56: 1318–1330.
29. Provost J, Gurev V, Trayanova N, Konofagou EE (2011) Mapping of cardiac electrical activation with electromechanical wave imaging: an in silico-in vivo reciprocity study. Heart Rhythm 8: 752–759.
30. Vigmond EJ, Hughes M, Plank G, Leon LJ (2003) Computational tools for modeling electrical activity in cardiac tissue. J Electrocardiol 36 Suppl: 69–74.
31. Panfilov AV, Keldermann RH, Nash MP (2005) Self-organized pacemakers in a coupled reaction-diffusion-mechanics system. Phys Rev Lett 95: 258104.
32. Isenberg G, Kazanski V, Kondratev D, Gallitelli MF, Kiseleva I, et al. (2003) Differential effects of stretch and compression on membrane currents and [Na+]c in ventricular myocytes. Prog Biophys Mol Biol 82: 43–56.
33. Morris CE (1990) Mechanosensitive ion channels. J Membr Biol 113: 93–107.
34. Li W, Gurev V, McCulloch AD, Trayanova NA (2008) The role of mechanoelectric feedback in vulnerability to electric shock. Prog Biophys Mol Biol 97: 461–478.
35. Kohl P, Day K, Noble D (1998) Cellular mechanisms of cardiac mechanoelectric feedback in a mathematical model. Can J Cardiol 14: 111–119.
36. Trayanova N, Li W, Eason J, Kohl P (2004) Effect of stretch-activated channels on defibrillation efficacy. Heart Rhythm 1: 67–77.
37. Larson C, Dragnev L, Trayanova N (2003) Analysis of electrically induced reentrant circuits in a sheet of myocardium. Ann Biomed Eng 31: 768–780.
38. Plonsey R, Barr RC (1989) Bioelectricity. New York: Plenum.
39. Cherry EM, Fenton FH (2004) Suppression of alternans and conduction blocks despite steep APD restitution: electrotonic, memory, and conduction velocity restitution effects. Am J Physiol Heart Circ Physiol 286: H2332–2341.
40. Cytrynbaum E, Keener JP (2002) Stability conditions for the traveling pulse: Modifying the restitution hypothesis. Chaos 12: 788–799.
41. Pollard AE, Burgess MJ, Spitzer KW (1993) Computer simulations of three-dimensional propagation in ventricular myocardium. Effects of intramural fiber rotation and inhomogeneous conductivity on epicardial activation. Circ Res 72: 744–756.
42. Sung D, Mills RW, Schettler J, Narayan SM, Omens JH, et al. (2003) Ventricular filling slows epicardial conduction and increases action potential duration in an optical mapping study of the isolated rabbit heart. J Cardiovasc Electrophysiol 14: 739–749.
43. Eckardt L, Kirchhof P, Monnig G, Breithardt G, Borggrefe M, et al. (2000) Modification of stretch-induced shortening of repolarization by streptomycin in the isolated rabbit heart. J Cardiovasc Pharmacol 36: 711–721.
44. White E, Le Guennec JY, Nigretto JM, Gannier F, Argibay JA, et al. (1993) The effects of increasing cell length on auxotonic contractions; membrane potential and intracellular calcium transients in single guinea-pig ventricular myocytes. Exp Physiol 78: 65–78.
45. Qu Z, Kil J, Xie F, Garfinkel A, Weiss JN (2000) Scroll wave dynamics in a three-dimensional cardiac tissue model: roles of restitution, thickness, and fiber rotation. Biophys J 78: 2761–2775.
46. Weiss JN, Qu Z, Chen PS, Lin SF, Karagueuzian HS, et al. (2005) The dynamics of cardiac fibrillation. Circulation 112: 1232–1240.
47. Girouard SD, Pastore JM, Laurita KR, Gregory KW, Rosenbaum DS (1996) Optical mapping in a new guinea pig model of ventricular tachycardia reveals mechanisms for multiple wavelengths in a single reentrant circuit. Circulation 93: 603–613.
48. Panfilov AV (2002) Spiral breakup in an array of coupled cells: the role of the intercellular conductance. Phys Rev Lett 88: 118101.
49. ten Tusscher KH, Panfilov AV (2003) Influence of nonexcitable cells on spiral breakup in two-dimensional and three-dimensional excitable media. Phys Rev E Stat Nonlin Soft Matter Phys 68: 062902.
50. Kuijpers NH, Potse M, van Dam PM, ten Eikelder HM, Verheule S, et al. (2011) Mechanoelectrical coupling enhances initiation and affects perpetuation of atrial fibrillation during acute atrial dilation. Heart Rhythm 8: 429–436.
51. Nishimura S, Kawai Y, Nakajima T, Hosoya Y, Fujita H, et al. (2006) Membrane potential of rat ventricular myocytes responds to axial stretch in phase, amplitude and speed-dependent manners. Cardiovasc Res 72: 403–411.
52. Franz MR, Cima R, Wang D, Profitt D, Kurz R (1992) Electrophysiological effects of myocardial stretch and mechanical determinants of stretch-activated arrhythmias. Circulation 86: 968–978.
53. Jie X, Gurev V, Trayanova N (2010) Mechanisms of mechanically induced spontaneous arrhythmias in acute regional ischemia. Circ Res 106: 185–192.